ASEAN Engineering Journal

Full Paper

OPTIMIZATION OF OPERATIONAL PARAMETERS TO ENHANCE SYNGAS YIELD AND SELECTIVITY IN THE GASIFICATION PROCESS WITHIN A FLUIDIZED BED REACTOR

Muhammad S. Khalid, Atha Hamzah, Yuswan Muharam*

Chemical Engineering Department, Faculty of Engineering, University of Indonesia, 16424, Depok, West Java, Indonesia

Article history
Received
16 July 2024
Received in revised form
13 November 2024
Accepted
07 July 2025
Published online
31 August 2025

*Corresponding author
muharam@che.ui.ac.id

Graphical abstract

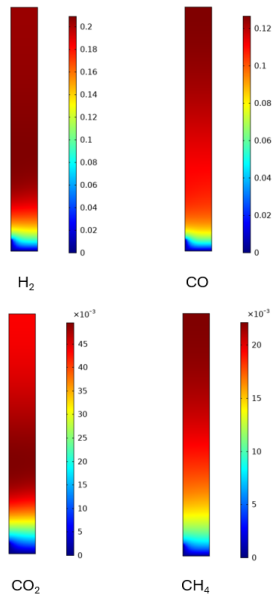

Abstract

One of the gasifiers used in the gasification process is the fluidized bed reactor. Determining the optimal process parameters for a fluidized bed reactor through direct experimentation is both time-consuming and costly. These challenges can be addressed through a computational fluid dynamics (CFD) based numerical approach. In this study, the Eulerian-Eulerian two-phase model coupled with kinetic model will be employed to predict the amount of product produced by chemical reaction. To achieve the best performance of the fluidized bed reactor and optimize the production of syngas, variations in temperature, airflow rate, biomass flow rate, and biomass humidity will be explored to determine the optimal operational conditions for syngas production and selectivity. The simulation results indicate that high-intensity reactions occur around the biomass feed, increasing the temperature in that region. Changes in process parameters influence syngas yield. H_2 yield enhanced 3% at 12 L/min air flow rate. Conversely H_2 production decreased at inlet air temperature 823 K due to consumed to produce CH_4. A high biomass feed rate extends retention time, thereby increasing the likelihood of secondary reactions that produce CO and CH_4. Additionally, high water content in the gasification process decreases CO production and increases CO_2 production.

Keywords: Optimization, Gasification, Fluidized Bed Reactor, Syngas, Computational Fluid Dynamics

1.0 INTRODUCTION

World population growth and rapid industrial development in the last few decades have led to increasing energy demand. Global energy consumption has increased from 141,326 TWh in 2010 to 178,899 TWh in 2022 [1]. Meanwhile fossil fuel is no longer sufficient to meet the demand due to their dwindling availability. Renewable and cleaner energy sources such biomass, tidal, wave, solar, wind, geothermal, etc. have been developed and explored to substitute the use of fossil fuel.

Biomass is an energy source that come from organic materials such plants or animals [2] [3]. Biomass considered as an energy source that has good availability since it consists of various wide range of materials and has low dependency on time like wind and solar energy that depend on climate and sun exposure [4]. Utilization biomass playing the important role on decarbonization since amount of carbon dioxide that it absorbs through its life cycle is the same as amount of carbon that release to the environment, so it considered as carbon neutral [5]. In present days, lignocellulosic materials such agriculture and forestry waste are preferable as biomass energy sources

since it does not disturb human's food supply [6]. Especially in Indonesia, where numerous plant species grows, biomass waste such wood waste from industrial and agriculture left out being degraded by nature. The amount of energy that can utilized from wood waste is estimated to reach 120 GJ per year [7]. Aside from its availability, its low content of sulfur and its heating value make wood has good potency as energy source [8]. To effectively utilized, wood can be processed through gasification, which convert biomass into valuable resources [9].

Gasification is a process that converts carbonaceous materials into gaseous materials called syngas which mainly consisted of H_2 dan CO. Earlier experimental research conducted by Maniatis et al [10] about wood gasification inside fluidized bed reactor found out that feedstock flowrate influenced the quality of syngas product, where the lack of air as gasification medium to the ratio of below 0.2 is not suitable to support the autothermal operation inside the reactor. Low air to biomass ratio in wood gasification was investigated by Bandara et al [11], where the 0.16 air to biomass ratio is still sufficient to completely convert char fraction. Research by Zhao et al [12] about sawdust gasification showed that the increase of reaction temperature from 700°C to 1000°C enhances the yield of H_2 and CO_2. Research conducted by Chen et al [13] on the effect of temperature and heating time to sawdust in a laboratory scale gasifier concluded that external heating could improve reactor performance, and cracking temperature at 700°C is preferable in economic point of view. Experiment about the influence of woodchip moisture conducted by Sommas & Suneerat [14] found out that the increase of moisture content up to 25.5% reducing temperature inside the reactor, which give the negative effect on reactor performance. It also mentioned that increase of moisture content increasing CO_2 production. The same result was also received by Pfeifer et al [15] where the high amount of water content in wood gasification led to the decrease of overall efficiency.

Fluidized bed gasifier is an efficient reactor in gasification process because it's excellent solid mixing and heat transfer [16] [17]. Moreover, fluidized bed also has the capability to scale-up and handle wide range of biomass [18] [19]. In order to determine the operational condition of fluidized bed gasifier, direct experiment may bring the accurate result, but the test will cost a lot of money and much time [9] [20]. Moreover, it is difficult to observe the behavior of material inside the fluidized bed gasifier due to the opaqueness of its wall. Those problems can be overcome through numerical approach based on computational fluid dynamics (CFD). CFD can visualize the flow of mass, energy, and momentum inside the gasifier. Through CFD, some adjustments to optimize the reactor performance are a lot easier and cheaper to carry out.

To simulate the gasification process, numerical methods based on CFD have been developed. In general, there are two types of CFD model that are utilized to compute the interaction between solid phase and gas phase. Eulerian-Lagrangian CFD model called Discrete Element Method (DEM) utilizes conventional Navier-Stokes equations to compute continuum phase and lagrange method to track solid particle behavior. Previous studies that utilize CFD-DEM to predict the influence of various operation parameters to the overall operational condition [21] [22] [23] [24]. This method is considered expensive since it requires a high specification computer to compute thousands or even millions of particles [24] [25]. On the hand, Eulerian-Eulerian model called Two Fluid Model (TFM) treats both fluid and solid phase as continuum. This method can simulate the gasification process with lower cost of computation since both solid and gas phase were computed using Navier-Stokes equations. TFM has been utilized to simulate gasification processes inside fluidized bed reactor with various types of biomasses such as rice husk [26], coffee husk [27] [28], peach stone and miscanthus [29].

In the present study, Eulerian-Eulerian two-phase model will be utilized to simulate mass, energy, and momentum balance inside the reactor. Meanwhile reaction kinetic model will be utilized to predict the amount of product produced by chemical reaction. To achieve an optimum fluidized bed performance and selection in syngas yield, variation of temperature, air flow rate, biomass flow rate, and biomass humidity will be simulated to get the optimum operational condition in producing syngas and selectivity.

2.0 METHODOLOGY

As previously mentioned, wood was chosen as gasification feedstock due to its availability and capability as syngas producer. Content of wood as obtained from proximate and ultimate analysis is represented in Table 1.

Table 1 Proximate and ultimate analysis [18]

	Content
Ultimate Analysis (wt%)	
C	47.41
H	6.12
N	0.2
Cl	0.05
S	0.01
O	45.00
Proximate analysis (wt%)	
Moisture	15.00
Volatile matter	83.80
Ash	1.16
Fixed Carbon	16.20

Biomass with a diameter of 0.5 mm is fed into the gasifier at a flow rate of 0.08 g/s. The gasification process takes place inside a lab-scale fluidized bed gasifier with a diameter of 4.445 cm and a height of 40 cm. Sand acts as inert material with a static height of 8 cm. Air is blown from the bottom of the reactor at a velocity of 11 cm/s. The simulation is conducted using a two-dimensional Euler-Euler two-phase model.

2.1. Drying

The rate of moisture release from the biomass expressed as [30]:

$$R_{\text{evp}} = \frac{Q_{\text{cr}}}{H_{\text{evp}}} \quad (1)$$

$$Q_{\text{cr}} = A_{\text{s}} h_{\text{s}} (T_{\text{g}} - T_{\text{s}}) \quad (2)$$

Where R_{evp} is drying rate, H_{evp} evaporation heat, Q_{cr} is absorbed heat by solid phase, A_{s} is particle surface area, T_{s} is solid phase temperature, and T_{g} is gas phase temperature.

2.2. Kinetics Model

The gasification kinetics model developed by Kumar and Paul [31] were used to predict the gasification yield. In the early stages of gasification, biomass containing $C_xH_yO_z$ components decomposes into simpler components such as char, volatiles, and condensable hydrocarbons. In this study, the gasification process is approached through the volatile break-up approach. The volatile break-up approach assumes that non-condensable gases such as H_2, CO, CO_2, H_2O, N_2, and S are packaged into a pseudo-gas phase called volatile. Then, the volatile gas decomposes into these gases through stoichiometric equilibrium as expressed in Equations (3) and (4), where *X1* to *X7* are the equilibrium constants for each species.

Biomass → Volatile + Char + Tar (3)

Volatile → $X1H_2 + X2CO + X3CO_2 + X4CH_4 + X5H_2O + X6N_2 + X7S$ (4)

Table 2 Kinetics model

Reaction	Reaction Equation	A	E (J mol^{-1})	Source
Water-gas Reaction	C + H_2O → CO + H_2	8.268	188200	[32]
Boudouard Reaction	C + CO2 → 2CO	12.2	144000	[32]
Partial Oxidation Reaction	2C + O2 → 2CO	147000	113000	[32]
Forward Water Gas Shift Reaction	CO + H2O → CO2 + H2	2.35e+10	12554	[33]
Reverse Water Gas Shift Reaction	CO2 + H2 → CO + H2O	1.785e+12	45544	[33]
Steam Reforming Reaction	CH4 + H2O→ CO + 3H2	3e+8	36150	[34]
CO Oxydation Reaction	CO + 0.5O2 → CO2	1.0e+10	126000	[34]
Hidrogenation Reaction	C + $2H_2$ → CH_4	8.8894e-06	19210	[34]

The Arrhenius equation is employed to calculate reaction rate constant.

$$k_i = A_i \exp\left(-\frac{E_i}{RT}\right) \quad (5)$$

Where A_i is pre-exponential factor and E_i is activation energy.

2.3. Transport Equations

To obtain an accurate model, the momentum, mass, and energy balances must be well defined. The momentum balance in this model is expressed in Equation (5) and Equation (6):

$$\rho(u_g \cdot \nabla)u_g = \nabla \cdot [-pl + \tau_g] + \rho_g g + \frac{F_m g}{\phi_g} + F_g \quad (6)$$

$$\rho(u_s \cdot \nabla)u_s = \nabla \cdot [-pl + \tau_s] + \rho_s g + \frac{F_m g}{\phi_s} \quad (7)$$

Where

$$\tau_g = (\mu_g + \mu_T)\left(\nabla u_g + (\nabla u_g)^T - \frac{2}{3}(\nabla \cdot u_g)l\right) - \frac{2}{3}\rho_g kl \quad (8)$$

$$\tau_s = (\mu_s + \mu_T)\left(\nabla u_s + (\nabla u_s)^T - \frac{2}{3}(\nabla \cdot u_s)l\right) - \frac{2}{3}\rho_s kl \quad (9)$$

Where ρ is density, u is velocity, p is pressure, l is reactor length, τ is shear stress, g is gravitation, μ is dynamic viscosity, F_m is interphase force, ϕ is porosity, k is kinetic energy, s subscript is solid phase, g subscript is gas phase, m subscript is solid-gas interphase, and T subscript is total. The Reynolds Averaged Navier-Stokes (RANS) turbulent model is applied to model the turbulent regime. The equation below uses the average density and velocity of the two phases in the turbulence model equation.

$$\rho_s = \phi_s \rho_s + (1 - \phi_s)\rho_g \quad (10)$$

$$u_m = \frac{(\phi_s u_s \rho_s + (1-\phi_s) u_g \rho_g)}{\phi_s \rho_s + (1-\phi_s)\rho_g} \quad (11)$$

The momentum balance boundary condition at the inlet is expressed in Equations (11) and Equations (12), where the inlet velocity is the same as the initial velocity for both the solid and gas phases.

$$u_g = u_{g0} \quad (12)$$

$$u_s = u_{s0} \quad (13)$$

The boundary condition at the outlet is expressed by Equations (13) to Equations (14), where the outlet pressure is equal to the initial pressure and there is no shear stress for both the gas and solid phases at the outlet, while n is vector operations.

$$p = p_0 \quad (14)$$

$$\tau_g n = 0 \quad (15)$$

$$\tau_s n = 0 \quad (16)$$

The no-slip wall condition is applied to the wall boundary, as stated in Equation (16) and Equation (17).

$$u_g \cdot n \quad (17)$$

$$u_s \cdot n \quad (18)$$

Mass balance used in this model expressed as:

$$\nabla \cdot (-D_{ig} \nabla c_{ig}) + u_{ig} \cdot \nabla c_{ig} = R_{ig} \quad (19)$$

$$\nabla \cdot (-D_{is} \nabla c_{is}) + u_{is} \cdot \nabla c_{is} = R_{is} \quad (20)$$

$$\frac{\partial c_i}{\partial t} - D_i \frac{\partial^2 c_i}{\partial x^2} - D_i \frac{\partial^2 c_i}{\partial y^2} + u_x \frac{\partial c_i}{\partial x} + u_y \frac{\partial c_i}{\partial y} = R_i + \frac{D_i}{x} \frac{\partial c_i}{\partial x} \quad (21)$$

Where D_i is the diffusion coefficient species i, C_i is concentration i, R_i is reaction rate species i, x is cartesian coordinate x, y is cartesian coordinate y, t is time. In drying and pyrolysis reactions, wet biomass produces water vapor while dry biomass decomposes into char and several gas species. Diffusion and convection mass transfer are modeled by two-

dimensional mass flow. To replicate cylindrical geometry, a three-dimensional cylindrical mass transfer equation model is adapted to a two-dimensional coordinate model expressed in Equation (20).

The change in species from the solid phase to the gas phase results in a variation in volumetric flow rate, thus the continuity equation can be expressed as:

$$\nabla\left(\phi u_{\mathrm{g}}\rho_{\mathrm{g}}\right) = S_{\mathrm{sg}} \tag{22}$$

$$(1-\phi)\rho_{\mathrm{s}}u_{\mathrm{s}} = -S_{\mathrm{sg}} \tag{23}$$

Where S_{sg} is gas produced from drying and pyrolysis reaction. While boundary condition is expressed in equation (24) and (25), outlet section is expressed in equation (26), and wall section is expressed in equation (27) and (28).

$$\mathrm{n}\cdot\left(-D_{\mathrm{ig}}\nabla c_{\mathrm{ig}} + u_{\mathrm{ig}}\right) = \mathrm{n}\cdot u_{\mathrm{g}}c_{0\mathrm{i}} \tag{24}$$

$$\mathrm{n}\cdot\left(-D_{\mathrm{is}}\nabla c_{\mathrm{is}} + u_{\mathrm{is}}\right) = \mathrm{n}\cdot u_{\mathrm{s}}c_{0\mathrm{i}} \tag{25}$$

$$\mathrm{n}\cdot D_{\mathrm{ig}}\nabla c_{\mathrm{ig}} = 0 \tag{26}$$

$$\mathrm{n}\cdot D_{\mathrm{ig}}\nabla c_{\mathrm{ig}} = 0 \tag{27}$$

$$\mathrm{n}\cdot D_{\mathrm{is}}\nabla c_{\mathrm{is}} = 0 \tag{28}$$

The energy balance governs the heat distribution within the system as expressed in Equation (29)

$$\rho C_{\mathrm{p}}u\cdot\nabla T + \nabla\cdot q = 0 \tag{29}$$

$$q = k_{\mathrm{eff}}\nabla T \tag{30}$$

$$k_{\mathrm{eff}} = \phi_{\mathrm{s}}k_{\mathrm{s}} + \left(1-\phi_{\mathrm{g}}\right)k_{\mathrm{g}} \tag{31}$$

Where C_p is heat capacity, T is temperature, q is heat flux, Q is the heat in the system, k is thermal conductivity, k_{eff} is the effective interphase conductivity. Boundary conditions in the energy balance are defined in Equation (31) for the inlet, where the energy flux is equal to the amount of heat generated by the enthalpy difference. No heat is transferred at the outlet, and the wall is insulated, so no flux condition is applied on either boundary as expressed in equation (32).

$$-\mathrm{n}\cdot q = \rho\Delta H u\cdot\mathrm{n} \tag{31}$$

$$-\mathrm{n}\cdot q = 0 \tag{32}$$

3.0 RESULTS AND DISCUSSION

Figure 1 depicts the reaction rate across the height of the reactor. While there are eight reactions involved in this study, only the most significant rates are displayed. The water-gas shift reaction occurs near the air inlet due to the separation of water content and the generation of carbon monoxide during the pyrolysis phase at the bottom of the reactor [35]. Carbon monoxide is produced during partial oxidation and the Boudouard reaction. Partial oxidation occurs due to char combustion, while the Boudouard reaction happens because carbon dioxide, resulting from carbon monoxide oxidation, further reacts with char. Another significant reaction is hydrogenation, which involves the reaction between char and hydrogen, producing methane. The height of the reactor affects the gas products from the gasification reaction. The continued reaction rate at the top of the reactor indicates that increasing the reactor height could facilitate further reactions due to the factor of residence time [36].

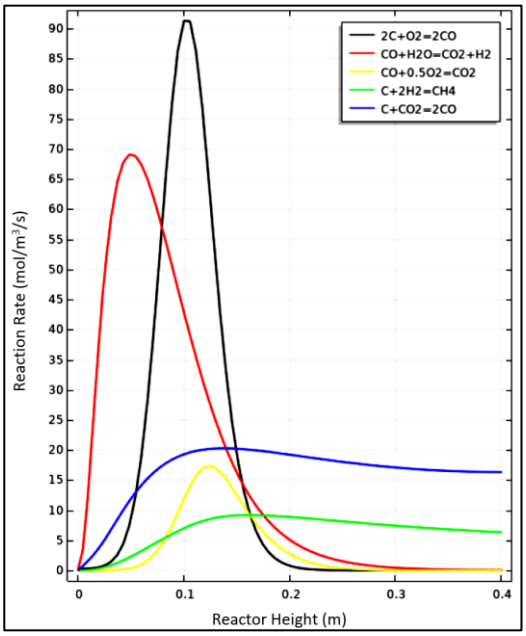

Figure 1 Reaction Rate Profile as a Function of Reactor Height

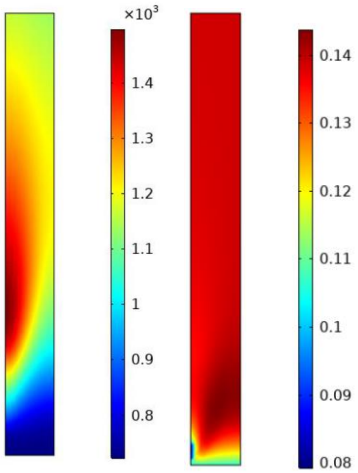

Figure 2 Temperature distribution (K) shows high intensity of exothermic reaction occur near biomass inlet [left]; The increase in velocity distribution (m/s) as consequence of interaction between biomass and gasifier flow [right]

The temperature distribution, illustrated in Figure 2, reveals that the highest temperatures are observed near the biomass feed inlet. As biomass enters the fluidized bed gasifier, it comes into contact with hot air, leading to its conversion into char, volatile compounds, and condensable gases. These materials undergo reactions with each other, consistent with Basu's explanation [9], that the gasification process is driven by exothermic

reactions in overall. This observation aligns with Figure 1, where the most intense reaction activity is concentrated around the biomass feed inlet.

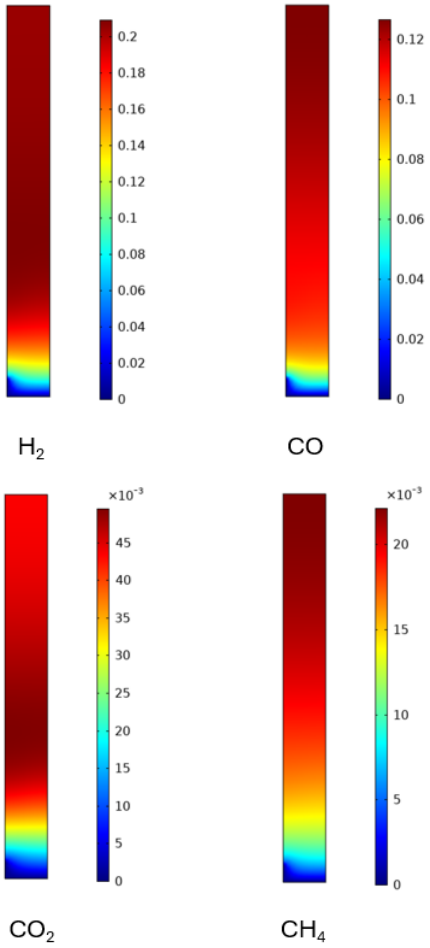

Figure 3 Mole Fraction Distribution of Hydrogen, Carbon Monoxide, Carbon Dioxide, and Methane as product of gasification process. The species distribution indicates that further reactions were occurring at the top part of reactor

Figure 3 depicts the mole distribution of each species involved in the gasification process. Hydrogen and carbon monoxide, serving as the primary products, exhibit higher mole fractions compared to carbon dioxide and methane, which are considered side products [3][9]. The mole fraction of hydrogen experiences a slight decrease towards the top of the reactor due to its reaction with char, resulting in methane generation. Conversely, the highest mole fraction of carbon monoxide is observed at the top of the reactor. While hydrogen is consumed with increasing reactor height, carbon monoxide is predominantly formed via the Boudouard reaction, as illustrated in Figure 1. Notably, carbon monoxide formation involves partial oxidation reactions near the biomass feed, although it is also subject to consumption through carbon monoxide oxidation reactions and the water-gas shift reaction.

Methane and carbon dioxide exhibit lower mole fractions compared to hydrogen and carbon monoxide, serving as side products in the gasification process. Methane's mole fraction increases towards the top of the reactor due to the hydrogenation of carbon monoxide. Meanwhile, carbon dioxide attains its highest mole distribution in the middle of the reactor but decreases towards the reactor's top. This decline is attributed to the oxidation of carbon monoxide, which forms carbon dioxide initially. Subsequently, carbon dioxide reacts further with char, producing carbon monoxide. Consequently, the mole fraction of carbon dioxide decreases at the top of the reactor due to its consumption in the Boudouard reaction.

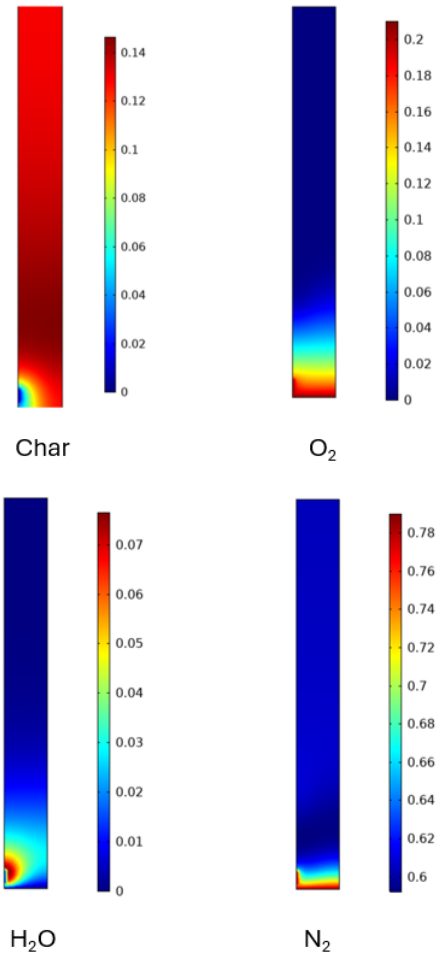

Figure 4 Mole fraction distribution of char, oxygen, water as reactant, while nitrogen as inert. High concentration of water at the inlet indicates a rapid evaporation by the hot air, and furthermore consumed by the reactions.

During the pyrolysis reaction, biomass decomposes into char and gas, thus lead to high amount of char present across the reactor. Subsequently, this char reacts with oxygen and water vapor, as detailed in the kinetic model presented in Table 2. Towards the top of the reactor, char is consumed primarily through hydrogenation reactions, which produce methane, and through reactions with carbon dioxide to generate carbon monoxide. These reactions contribute to the decrease in char mole fraction at the top of the reactor, as illustrated in Figure 4.

In Figure 4, it can be observed that the oxygen concentration decreases after leaving the air inlet. This reduction in oxygen concentration indicates that oxidation reactions have occurred around the biomass feeder. The gasification process typically occurs with a low amount of oxygen, resulting in the oxygen being consumed by the reaction.

Similarly, the water concentration decreases as the drying process separates the water content from the biomass. The water then reacts with char to produce carbon monoxide and hydrogen. Additionally, water reacts with carbon monoxide to produce carbon dioxide and hydrogen, while some water also reacts with methane to produce carbon monoxide and hydrogen. This phenomenon explains the high-water content around the biomass feeder and the low concentration at the outlet of the reactor.

Nitrogen is considered an inert gas in volatile break up approach [31]. Its high concentration at the inlet is attributed to the use of air as the gasification medium, which comprises 78% nitrogen. Biomass decomposition produces more gas, resulting in a relative decrease in nitrogen concentration at the top of the reactor.

Table 3 Air flow rate and syngas yield

Flow Rate (L/min)	Yield (Mole Fraction)			
	CO	CO_2	H_2	CH_4
8	0.32099	0.1111	0.50405	0.063852
9	0.32	0.11036	0.51042	0.059228
10	0.31923	0.10983	0.51511	0.055825
11	0.3186	0.10946	0.51872	0.053225
12	0.31808	0.10918	0.52157	0.051175

Table 4 The effect of biomass feed rate on syngas yield

Biomass Density (vol%)	Yield (Mole Fraction)			
	CO	CO_2	H_2	CH_4
0.08	0.2929	0.1221	0.5466	0.0385
0.1	0.3069	0.1152	0.5328	0.0452
0.12	0.3192	0.1098	0.5151	0.0558
0.14	0.3315	0.1060	0.4912	0.0712
0.16	0.3437	0.1038	0.4613	0.0912

Table 3 represents the impact of different air flow rates (dm^3/min) on syngas yield. As depicted in the figure, hydrogen production increases with higher air flow rates. Lower air flow rates provide an opportunity for char and hydrogen to produce methane as represented in Figure 1. Conversely, higher air flow rates reduce the likelihood of hydrogen reacting with char, as the increased momentum carries the hydrogen more swiftly to the top of the reactor. Hence, maximum hydrogen production can be approached at the operational condition of 12 L/min air flow rate. In contrary with hydrogen production, other products such carbon monoxide, carbon dioxide, and methane production reach the maximum yield at lower air flow rate. As mentioned before, that low air flow rate provides the opportunity for the species to react further. At air flow rate 8 L/min, the likelihood of carbon monoxide oxidation and Boudouard reaction are getting higher, thus leading to the higher yield of carbon monoxide and carbon dioxide.

Table 4 represents the influence of biomass feed rate on the yield of syngas. Biomass feed rate is relative to the amount of gasification medium. A lower biomass feed rate relatively increases the amount of oxygen available for the oxidation reaction. Meanwhile, a higher biomass feed rate makes the oxygen increasingly limited and extends the retention time due to the low magnitude of momentum. Therefore, at biomass 0.16% volume, hydrogen production significantly decreased, while methane production increased. The extent of retention time increases the likelihood of hydrogenation reaction which produces methane as its product. Conversely, hydrogen production maximized at 0.08% volume due to low retention time. The retention time also takes effect on carbon monoxide and carbon dioxide production. The extent of retention time contributes to carbon monoxide generation through Boudouard reaction. Hence biomass feed rate at 0.16% of volume maximize carbon monoxide production. While in the contrary, carbon dioxide production decreased due to consumed during Bouduoard reaction as represent in Figure 1. The experiment conducted by Emiola-Sadiq et al [39] also find similar findings, where high biomass feed rate increases the retention time, which led to the decrease of hydrogen production. Furthermore, the study also reported that too low biomass feed rate caused excess fluidization which led to decreasing fluidized bed efficiency. This finding met the agreement with the study conducted by Gil et al [41] and Pinto et al [42]. With the result reported in this paper, it's proven that the adjustment between biomass feed rate and air flow rate is essential to gasification reactor performance.

Table 5 Influence of inlet air temperature and syngas yield

Air Temperature (K)	Yield (Mole Fraction)			
	CO	CO_2	H_2	CH_4
623	0.3166	0.1083	0.5291	0.0459
673	0.3181	0.1091	0.5220	0.0509
723	0.3192	0.1098	0.5151	0.0558
773	0.3202	0.1106	0.5086	0.0606
823	0.3211	0.1114	0.5023	0.0651

Table 6 Influence of biomass humidity to the yield of syngas

Water Content (wt%)	Yield (Mole Fraction)			
	CO	CO_2	H_2	CH_4
13.5	0.34588	0.08948	0.51305	0.05160
16	0.33225	0.09987	0.51421	0.05367
18.5	0.31923	0.10983	0.51511	0.05583
21	0.30642	0.11966	0.51584	0.05808
23.5	0.29350	0.12959	0.51645	0.06047

The effect of air inlet temperature on syngas yield is represented in Table 5. Hydrogen production decreases with increasing air temperature, which can be observed that the highest yield of hydrogen can be achieved with 623 K of air inlet temperature. As shown in Table 2, water gas shift reaction is reversible reaction, where the forward reaction is an exothermic reaction [9], hence the peaked temperature due to heat of reaction will promote the backward water gas shift reaction and reducing hydrogen product as consequence. In contrary, higher

temperatures from the inlet air promote methane formation, since volatile production increased during pyrolysis at higher temperature [37] [38]. The increase in volatile production at high temperature also increase the likelihood of hydrogenation reaction. As consequence, inlet air temperature 823 K significantly maximizes methane production. In contrast, carbon monoxide and carbon dioxide production just slightly increased by the increase of temperature, even though both species yield also maximized at air temperature 823 K.

Biomass humidity influences the water content in the gasification process. As shown in Table 6, an increase in water content escalates the production of hydrogen due to the water-gas reaction and water-gas shift reaction. Hence, hydrogen production can be maximized at 23.5% water content. As presented in Figure 1, water immediately reacts after being separated from the biomass by the drying process around the biomass feed, thus led to the increase of hydrogen production. Hydrogen reacts with char through the hydrogenation reaction, which lead to the maximum yield of methane at 23.5% water content. High water content provides the amount of water to produce carbon dioxide through water gas shift reaction, which explains the maximum carbon dioxide production at water content 23.5%. In contrary, carbon monoxide consumed during water gas shift reaction, which explain why the carbon monoxide production maximized during water content 13.5%.

The effect of water content to syngas production in the current study has similar result with study conducted by Ismail et al [28] where the higher water content in coffee husk also enhances the hydrogen, methane, and carbon dioxide production. The study also found out that higher amount of water causes the decrease of reactor performance, since large amount of water content requires higher energy to the evaporation process, which has the agreement with the study conducted by Kaewluan & Pipatmanomai [14] and Pfeifer et al [15]. The study [28] was performed in a fixed reactor temperature to prevent the agglomeration due to high number of potassium oxide in coffee husk ash [40]. In this study, the inlet air act as the main heat source for the reactor instead of heat exchanger coiled around the reactor wall. The heat that continuously flows from the inlet will directly perform the evaporation process and overcome the heat loss during this process. Besides, heat generated by exothermic reaction can provide heat that is required to perform the autothermal. The temperature peak does not much affect the reactor performance since low content of potassium oxide inside the wood ash makes it insensitive to agglomeration [40]. Therefore, the utilization of wood biomass can increase the acceptable moisture content that can proceed within the fluidized bed gasifier, although the level of humidity needs to be handled with caution since the high number of humidity can decrease the amount of heat required for the process [14].

4.0 CONCLUSION

In the present study a CFD based numerical approach was utilized to model the gasification process inside fluidized bed reactor. From the simulation it can be known that the most significant rate of reaction occurs in the area around biomass feed, with the highest magnitude of char oxidation reaction. Distribution of temperature shows that the highest temperature magnitude occurs around the area where char oxidation takes place. CFD simulation is able to show the number of species that consumed and produced during gasification process through mole fraction distribution along the reactor.

Changes in operational parameters influence the yield of syngas produced. Changes in operational parameters influence the yield of syngas produced. Hydrogen production can be optimized at 12 L/min air flow rate, with 623 K air inlet temperature, 0.08% biomass volume, and 23.5% water content. Carbon dioxide yield optimized at 8 L/min air flow rate, 0.16% biomass volume, and 13.5% water content, while the influence of temperature doesn't significantly affect carbon monoxide production. Methane as the co-product can be intensified at 8 dm3/min air flow rate, 823 K air inlet temperature, 0.16% biomass volume, and 23.5% water content. Carbon dioxide production enhanced at operational condition 8 L/min air flow rate, 0.16% biomass volume, and 13.5% water content.

Acknowledgement

The research was supported by the program of Hibah Publikasi Terindeks Internasional (PUTI) Q1 2024–2025, grant number NKB-548/UN2.RST/HKP.05.00/2024, which was granted by the Universitas Indonesia in 2024.

Conflicts of Interest

The author(s) declare(s) that there is no conflict of interest regarding the publication of this paper

References

[1] Ritchie, H., P. Rosado, and M. Roser. 2024. Our World in Data. https://ourworldindata.org/energy-mix#article-citation Retrieve on: February 2024

[2] Loppinet-Serani, Anne, Cyril Aymonier, and François Cansell. 2008. Current and Foreseeable Applications of Supercritical Water for Energy and the Environment. *ChemSusChem* 1(6): 486–503. DOI: 10.1002/cssc.200700167.

[3] Brown, R. C. 2011. *Thermochemical Processing of Biomass: Conversion into Fuels, Chemicals and Power*. Wiltshire: John Wiley & Sons.

[4] Singh, S. V, Z. Ming, P. S. Fennell, N. Shah, and E. J. Anthony. 2017. Progress in Biofuel Production from Gasification. *Progress in Energy and Combustion Science* 189–248. DOI: 10.1016/j.pecs.2017.04.001.

[5] Saidur, R., E. Abdelaziz, A. Demirbas, M. Hossain, and S. Mekhilef. 2011. A Review on Biomass as a Fuel for Boilers. *Renewable and Sustainable Energy Reviews* 2262–89. DOI: 10.1016/j.rser.2011.02.015.

[6] Mong, G. R., C. T. Chong, J. H. Ng, W. W. Chong, H. C. Ong, and M. V. Tran. 2021. Multivariate Optimisation Study and Life Cycle Assessment of Microwave-Induced Pyrolysis of Horse Manure for Waste Valorisation and Management. *Energy.* 216. DOI: 10.1016/j.energy.2020.119194

[7] Yana, S., M. Irhamni Nizar, and D. Mulyati. 2022. Biomass Waste as a Renewable Energy in Developing Bio-Based Economies in Indonesia: A Review. *Renewable and Sustainable Energy Reviews* 160. DOI: 10.1016/j.rser.2022.112268.

[8] Nukman, and R. Sipahutar. 2015. The Potential of Biomass from Wood, Leaves, and Grass as Renewable Energy Sources in South Sumatera, Indonesia. Energy Sources, Part A: Recovery, Utilization. *And Environmental Effects* 37(24): 2710–15. DOI: 10.1080/15567036.2012.738286.

[9] Basu, P. 2010. *Biomass Gasification and Pyrolysis*. Cambridge: Academic Press.

[10] Maniatis, K., A. Bridgwater, and A. Buekens. 1988. Fluidized Bed Gasification Of Wood. *Research in Thermochemical Biomass Conversion* 1094–1105. DOI: 10.1007/978-94-009-2737-7_83.

[11] Bandara, J. C., R. Jaiswal, H. K. Nielsen, B. M. Moldestad, and M. S. Eikeland. 2021. "Air Gasification of Wood Chips, Wood Pellets and Grass Pellets in a Bubbling Fluidized Bed Reactor." *Energy.* 233. DOI: 10.1016/j.energy.2021.121149.

[12] Zhao, Y., S. Sun, H. Zhou, R. Sun, H. Tian, J. Luan, and J. Qian. 2010. "Experimental Study on Sawdust Air Gasification in an Entrained-Flow Reactor." *Fuel Processing Technology* 910–14.

[13] Chen, G., J. Andries, Z. Luo, and H. Spliethoff. 2003. "Biomass Pyrolysis/Gasification for Product Gas Production: The Overall Investigation of Parametric Effects." *Energy Conversion and Management.* 44(11): 1875-1884. DOI: 10.1016/S0196-8904(02)00188-7

[14] Kaewluan, S., and S. Pipatmanomai. 2011. "Gasification of High Moisture Rubber Woodchip with Rubber Waste in a Bubbling Fluidized Bed." *Fuel Processing Technology* 92(3): 671–77. DOI: 10.1016/j.fuproc.2010.11.026.

[15] Pfeifer, C., S. Koppatz, and H. Hofbauer. 2011. "Steam Gasification of Various Feedstocks at a Dual Fluidised Bed Gasifier: Impacts of Operation Conditions and Bed Materials." *Biomass Conversion and Biorefinery* 1: 39–53.

[16] Thoharudin, Yi-Shun Chen, and Shu-San Hsiau. 2020. "Numerical Studies on Fast Pyrolysis of Palm Kernel Shell in a Fluidized Bed Reactor." *IOP Conference Series: Materials Science and Engineering* 874(1): 012033. DOI: 10.1088/1757-899X/874/1/012033.

[17] Diba, Mst Farhana, Md Rezwanul Karim, and Jamal Naser. 2022. "CFD Modelling of Coal Gasification in a Fluidized Bed with the Effects of Calcination under Different Operating Conditions." *Energy* 239: 122284. DOI: 10.1016/j.energy.2021.122284.

[18] Arora, Pratham, Andrew F. A. Hoadley, Sanjay M. Mahajani, and Anuradda Ganesh. 2017. Compartment Model for a Dual Fluidized Bed Biomass Gasifier. *Chemical Engineering Research and Design* 117: 274–86. DOI: 10.1016/j.cherd.2016.10.025.

[19] Kushwah, A., T. R. Reina, and M. Short. 2022. Modelling Approaches for Biomass Gasifiers: A Comprehensive Overview. *Science of The Total Environment* 834:155243. DOI: 10.1016/j.scitotenv.2022.155243.

[20] Yang, W. C. 2003. *Handbook Of Fluidization And Fluid-Particle Systems*. New York: Marcel Dekker.

[21] Pandey, Bhoopendra, Yogesh K. Prajapati, and Pratik N. Sheth. 2022. CFD Analysis of the Downdraft Gasifier Using Species-Transport and Discrete Phase Model. *Fuel* 328: 125302. DOI: 10.1016/j.fuel.2022.125302.

[22] Lian, Guoqing, and Wenqi Zhong. 2023. Coupling CFD-DEM with Cohesive Force and Chemical Reaction Sub-Models for Biomass Combustion in a Fluidized Bed. *Fuel* 350: 128858. DOI: 10.1016/j.fuel.2023.128858.

[23] Du, Shaohua, Jiahao Wang, Yaxiong Yu, and Qiang Zhou. 2023. Coarse-Grained CFD-DEM Simulation of Coal and Biomass Co-Gasification Process in a Fluidized Bed Reactor: Effects of Particle Size Distribution and Operating Pressure. *Renewable Energy* 202: 483–98. DOI: 10.1016/j.renene.2022.11.073.

[24] Wang, Qinggong, Hairui Yang, Yuqing Feng, Peter J. Witt, Junfu Lu, Weidi Yin, Qing Liu, and Lubin Wei. 2015. Numerical Study of the Effect of Operation Parameters on Particle Segregation in a Coal Beneficiation Fluidized Bed by a TFM–DEM Hybrid Model. *Chemical Engineering Science* 131: 256–70. DOI: 10.1016/j.ces.2015.03.063.

[25] Yin, Weijie, Shuai Wang, Kai Zhang, and Yurong He. 2020. Investigation of Oxygen-Enriched Biomass Gasification with TFM-DEM Hybrid Model. *Chemical Engineering Science* 211: 115293. DOI: 10.1016/j.ces.2019.115293.

[26] Raza, N., and M. Ahsan. 2024. Influence of Distributor Plate Design on Mixing Characteristics of Rice Husk Biomass in a Bubbling Fluidized Bed Gasifier: An Experimental and CFD Study. *Fuel* 358. DOI: 10.1016/j.fuel.2023.129893

[27] Couto, Nuno, Valter Silva, Eliseu Monteiro, Paulo Brito, and Abel Rouboa. 2015. Using an Eulerian-Granular 2-D Multiphase CFD Model to Simulate Oxygen Air Enriched Gasification of Agroindustrial Residues. *Renewable Energy* 77: 174–81. DOI: 10.1016/j.renene.2014.11.089.

[28] Ismail, Tamer M., M. Abd El-Salam, Eliseu Monteiro, and Abel Rouboa. 2016. Eulerian – Eulerian CFD Model on Fluidized Bed Gasifier Using Coffee Husks as Fuel. *Applied Thermal Engineering* 106: 1391–1402. DOI: 10.1016/j.applthermaleng.2016.06.102.

[29] Ismail, Tamer M., M. Abd El-Salam, Eliseu Monteiro, and Abel Rouboa. 2018. Fluid Dynamics Model on Fluidized Bed Gasifier Using Agro-Industrial Biomass as Fuel. *Waste Management* 73: 476–86. DOI: 10.1016/j.wasman.2017.06.018.

[30] Bruch, C. 2003. Modelling Wood Combustion under Fixed Bed Conditions⋆. *Fuel* 82(6): 729–38. DOI: 10.1016/S0016-2361(02)00296-X.

[31] Kumar, Umesh, and Manosh C. Paul. 2019. CFD Modelling of Biomass Gasification with a Volatile Break-up Approach. *Chemical Engineering Science* 195: 413–22. DOI: 10.1016/j.ces.2018.09.038.

[32] Xie, Jun, Wenqi Zhong, Baosheng Jin, Yingjuan Shao, and Hao Liu. 2012. Simulation on Gasification of Forestry Residues in Fluidized Beds by Eulerian–Lagrangian Approach. *Bioresource Technology* 121: 36–46. DOI: 10.1016/j.biortech.2012.06.080.

[33] Nakod, P. 2013. Modeling and Validation of Oxy-Fired and Air-Fired Entrained Flow Gasifiers. *International Journal of Chemical and Physical Sciences* 2: 2319–6602.

[34] Gómez-Barea, A., and B. Leckner. 2010. Modeling of Biomass Gasification in Fluidized Bed. *Progress in Energy and Combustion Science* 36(4): 444–509. DOI: 10.1016/j.pecs.2009.12.002.

[35] Ravi, M.R., Kohli, S. 2018. Thermodynamics and Kinetics of Gasification. In: De, S., Agarwal, A., Moholkar, V., Thallada, B. (eds) Coal and Biomass Gasification. Energy, Environment, and Sustainability. Springer: Singapore. DOI: 10.1007/978-981-10-7335-9_2

[36] Siedlecki, Marcin, Wiebren De Jong, and Adrian H.M. Verkooijen. 2011. Fluidized Bed Gasification as a Mature and Reliable Technology for the Production of Bio-Syngas and Applied in the Production of Liquid Transportation Fuels—A Review" *Energies* 4(3): 389-434. DOI: 10.3390/en4030389

[37] Lan, W., Chen, G., Zhu, X., Wang, X., Wang, X., & Xu, B. 2019. "Research on the characteristics of biomass gasification in a fluidized bed". *Journal of the Energy Institute*, 92(3): 613–620. DOI: 10.1016/j.joei.2018.03.011

[38] Emiola-Sadiq, T., Zhang, L., Dalai, A., Gerspacher, R., Campbell, B., & Evitts, R. 2024. "Parametric and hydrodynamics studies on gasification performance of biomass pellets in a pilot-scale fluidized bed gasifier." *Biomass Conversion and Biorefinery*, 14(14): 16339–16361. DOI: 10.1007/s13399-022-03716-2

[39] Emiola-Sadiq, T., Zhang, L., Dalai, A., Gerspacher, R., Campbell, B., & Evitts, R. 2024. "Parametric and hydrodynamics studies on gasification performance of biomass pellets in a pilot-scale fluidized bed gasifier." *Biomass Conversion and Biorefinery*, 14(14): 16339–16361. DOI: 10.1007/s13399-022-03716-2

[40] George, J., Arun, P., & Muraleedharan, C. 2019. "Experimental investigation on co-gasification of coffee husk and sawdust in a bubbling fluidised bed gasifier." *Journal of the Energy Institute*, 92(6): 1977–1986. DOI: 10.1016/j.joei.2018.10.014

[41] Gil, J., Corella, J., Aznar, M. P., & Caballero, M. A. 1999. "Biomass gasification in atmospheric and bubbling fluidized bed: Effect of the type of gasifying agent on the product distribution." *Biomass and Bioenergy*, *17*(5): 389–403. DOI: 10.1016/S0961-9534(99)00055-0

[42] Pinto, F., André, R., Miranda, M., Neves, D., Varela, F., & Santos, J. 2016. "Effect of gasification agent on co-gasification of rice production wastes mixtures." *Fuel*, *180*: 407–416. DOI: 10.1016/j.fuel.2016.04.048